Biol. Cybern. 57, 257–274 (1987)

Biological Cybernetics

The Control of Hand Equilibrium Trajectories in Multi-Joint Arm Movements

T. Flash

Department of Brain and Cognitive Sciences, Massachusetts Institute of Technology, Cambridge, MA 02139, USA and Department of Applied Mathematics, Weizmann Institute of Science, Rehovot 76100, Israel

Abstract. According to the *equilibrium trajectory hypothesis*, multi-joint arm movements are achieved by gradually shifting the hand equilibrium positions defined by the neuromuscular activity. The magnitude of the force exerted on the arm, at any time, depends on the difference between the actual and equilibrium hand positions and the stiffness and viscosity about the equilibrium position. The purpose of this paper is to test the validity and implications of this hypothesis in the context of reaching movements. A mathematical description of the behavior of an arm tracking the equilibrium trajectory was developed and implemented in computer simulations. The joint stiffness parameters used in these simulations were derived from experimentally measured static stiffness values. The kinematic features of hand equilibrium trajectories which were derived from measured planar horizontal movements gave rise to the suggestion that the generation of reaching movements involves explicit planning of spatially and temporally invariant hand equilibrium trajectories. This hypothesis was tested by simulating actual arm movements based on hypothetical equilibrium trajectories. The success of the predicted behavior in capturing both the qualitative features and the quantitative kinematic details of the measured movements supports the equilibrium trajectory hypothesis. The control strategy suggested here may allow the motor system to avoid some of the complicated computational problems associated with multi-joint arm movements.

1 Introduction

Arm movements aimed at stationary or moving targets are common in the motor repertoire of primates. Yet little is known how the brain uses spatiovisual information concerning the locations of objects for the generation of reaching movements and how it controls the different neural, muscular, and skeletal structures involved in the formation of arm trajectories (Georgopoulos 1986).

In studying the kinematic features of reaching movements it is important to distinguish between *path* and *trajectory*. The term path refers to the sequence of positions that the hand follows in space; trajectory is the time sequence of movement along the path. In what coordinate frame is the trajectory planned? The tendency of subjects to generate roughly straight hand paths with bell-shaped speed profiles in unconstrained point-to-point movements in the horizontal plane indicates that planning takes place in terms of hand trajectories rather than joint rotations, (Morasso 1981). In order to produce desired hand trajectories appropriate joint torques must be generated. The derivation of joint-torques requires transforming hand trajectory plans into joint rotations, and "computing" joint torques by "solving" the second-order nonlinear dynamic equations of motion. For multi-joint arms, there exist significant inertial dynamic interactions between the moving skeletal segments (Hollerbach and Flash 1982), and several muscles pull across more than one joint. Clearly, these complexities raise new control problems that do not exist in the single-joint case.

The explicit use of the spring-like properties of muscles may allow the system to circumvent the complex dynamic, kinematic and force distribution problems involved in the control of human multi-joint arm movements (Hogan 1985). By specifying a particular pair of torque-angle curves for the agonist-antagonist muscle groups acting on the limb, the equilibrium position for the limb and the stiffness about the joint can be determined (Asatryan and Feldman 1965; Feldman 1966; Bizzi et al. 1976; Nichols and Houk 1976; Hoffer and Andreassen 1981). Although it was initially suggested that motion is achieved simply through an abrupt shift of the equilib-

rium point to the final position (Bizzi et al. 1976; Polit and Bizzi 1979; Feldman 1980; Kelso and Holt 1980) recent studies of monkey elbow movements have indicated that the CNS generates control signals which define a series of equilibrium positions and not merely the final position (Bizzi et al. 1982, 1984). Similarly, Feldman (1974) suggested that the CNS may use the strategy of gradually shifting the equilibrium in order to control the velocity of movement.

In the context of a multi-joint system, the equilibrium position of the hand is established by the interaction of the elastic forces generated by the arm muscles (Mussa-Ivaldi et al. 1985). According to the *equilibrium trajectory hypothesis* for multi-joint arm motions, movements are achieved by gradually shifting the hand equilibrium positions between the movement end-points (Hogan 1985). Muscle visco-elastic forces propel the arm along the trajectory. Since in this control scheme the hand tracks its equilibrium point as it is moved in time, explicit torque computations are obviated. The appeal of this idea results from the theoretical simplicity of this control strategy compared to other control schemes (such as those derived from robotics).

The purpose of this work is to test the validity and implications of the equilibrium trajectory hypothesis in the context of reaching movements and to make concrete suggestions as to what kind of hand equilibrium trajectories are planned by the CNS and how the system specifies the time-histories of joint stiffnesses and viscosities. The results from this study indicate that a common equilibrium trajectory program may underlie the generation of a large class of movements. Our results also suggest that the hand stiffness field during motion may have similar characteristics to those observed for the static field.

2 Experimental Observations

2.1 Reaching Movements

Arm movements were measured with a pantograph gripped by a seated subject and moved in a horizontal plane between specified targets (Fig. 1 A). Shoulder movement of subjects was restrained and the wrist was immobilized by bracing. The position of the pantograph handle was determined from potentiometers located at the joints of the mechanical linkage and the shoulder joint angles were found using simple trigonometric calculations. Six LED targets (T_1 to T_6) were mounted on a plexiglass cover just above the apparatus. The distances between the targets ranged between 20 to 40 cm. The subjects were instructed to move the pantograph handle at various speeds between the targets as described in Hollerbach and Flash (1982).

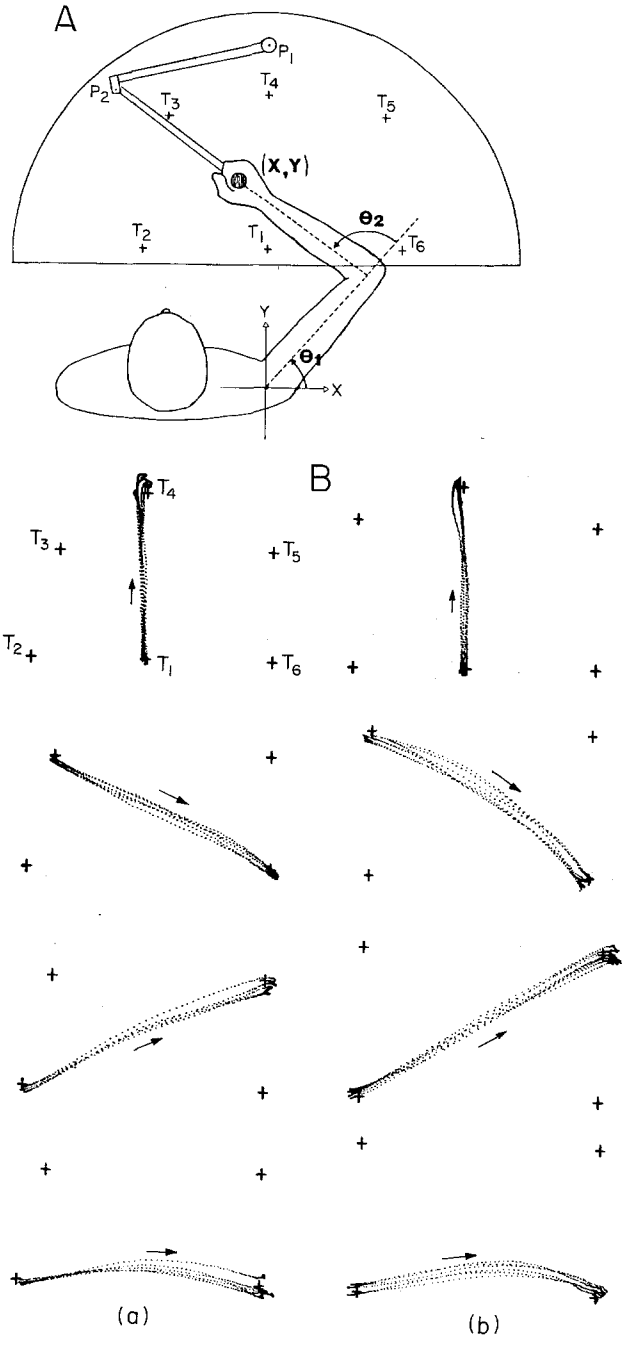

Fig. 1. **A** Experimental apparatus for measuring arm trajectories in the horizontal plane. **B** Sets of hand paths containing movements generated between different pairs of targets within one session. (*a*) Subject 1. (*b*) Subject 2

Movement durations ranged between 0.4 and 1.0 s. Visual information about the arm location was eliminated by darkening the room and no explicit instructions were given regarding the type of path between targets or end-point accuracy. No feedback of results was given to the subjects. Three subjects were tested.

The kinematic features of unconstrained planar point-to-point movements have been discussed in detail elsewhere (Morasso 1981; Abend et al. 1982). For present purposes the data may be condensed into a few key observations: The hand paths of all reaching movements in the horizontal plane are roughly straight independently of the workspace region in which the movement is performed. The joint velocity traces vary widely, while the hand velocity profile is always roughly bell-shaped and is invariant under changes in the speed, amplitude, end-points and direction of the movement. However, in describing the qualitative similarities between movements performed in different parts of the workspace, the more fine-grained details seen in real movements were previously overlooked. As can be seen from Fig. 1B, the hand paths are not ideally straight and the exact nature of movement curvature seems to depend on the region within the workspace in which the movement is generated. Similar patterns of trajectory deviations from straight paths can be found in different subjects while for the same subject, in movements generated on consecutive trials, the hand paths seem to follow roughly parallel lines. Notice also the presence of little hooks as the hand approaches the target.

2.2 *The Static Stiffness Field*

The hand stiffness field during two-joint arm posture has been recently measured by Mussa-Ivaldi et al. (1985) by applying servo-displacements to the hand while subjects maintained a given posture and measuring the restoring forces exerted on the hand at the displaced positions when the hand came to rest and before voluntary reaction. By analyzing the force and displacement data, the four elements of the hand stiffness matrix were numerically estimated. By evaluating the conservative and non-conservative components of the hand elastic field, it was established that the stiffness field is nearly curl free, i.e. the stiffness matrix is nearly symmetric, and hence the behavior of the system is predominantly springlike. These investigators also chose to represent the hand stiffness field graphically as an ellipse, which for a conservative field can be characterized by three independent parameters. The *orientation* is defined as the angle between the ellipse's major axis and the x axis of a laboratory fixed coordinate system, giving the direction in which the hand is maximally stiff. The *shape* parameter describes the ratio between the major and minor principal axes and the *size* corresponds to the area of the ellipse.

Typical stiffness ellipses for two subjects at fifteen different positions in the horizontal plane are shown in Fig. 2. As this figure indicates, the orientation of the hand stiffness field is roughly polar for most of the

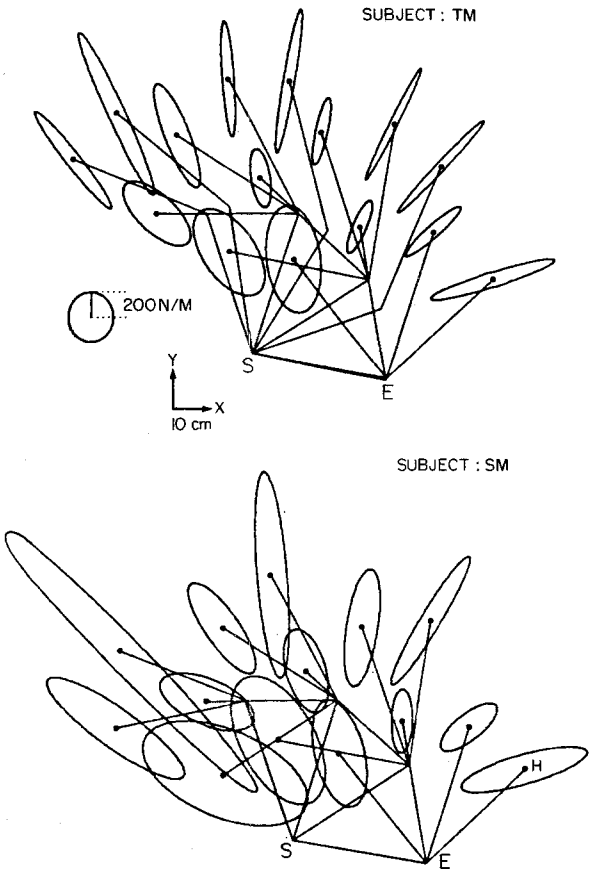

Fig. 2. Hand stiffness ellipses obtained from two subjects during the postural task. Each ellipse was derived by regression on about 60 force and displacement vectors. The upper arm and forearm represented by two line segments (*S–E*) and (*E–H*), respectively, and the ellipses are placed on the hand (*H*). The calibration for the stiffness is provided by the circle to the left, which represents an isotropic hand stiffness of 300 N/m

hand locations in the plane, i.e. the major axis of the stiffness ellipse is directed away from the body along the radial axis of a polar coordinate system whose origin is located at the shoulder. There exists also a slight but significant counterclockwise rotation of the stiffness ellipse as the hand is moved more proximally. Along the proximal-distal direction there is predominantly a change in the ellipse shape and the stiffness field becomes less isotropic as the hand is moved more distally. The shape and orientation of the stiffness ellipse at any hand location were found to be invariant over subjects and over time. The size of the stiffness field was found to vary substantially among subjects and over time. Using simple geometrical transformations (see Appendix A) joint stiffness matrices were derived from the corresponding hand stiffness matrices and the values of the joint stiffness coefficients were found to change under changes in hand position. Mussa-Ivaldi et al. (1985) also investigated the ability

of subjects to produce voluntary and adaptive changes in the stiffness field. When a disturbance force acting along a certain direction was imposed on the hand, the overall size of the stiffness ellipse increased by more than a factor of four but only minor changes occurred in the orientation and shape of the stiffness field. A more thorough inspection of their data (Mussa-Ivaldi et al. 1985; Fig. 12, p. 2741) reveals, however, that the value of the stiffness ellipse shape parameter could become 1.5–2 times as large as its value during normal posture. In a subsequent work Flash and Mussa-Ivaldi (1984, and in preparation) investigated the causes for the observed regularities of the hand stiffness field. The main results from this analysis will be presented in Sect. 4.1.2 below.

3 Mathematical Modelling

In the computer simulations presented here the arm was treated as a simple planar mechanism made of two uniform rigid cylinders, rotating in the plane as shown in Fig. 1A. The expression for the vector of resultant shoulder and elbow joint torques, required to drive the arm along any given trajectory is

$$\mathbf{n} = I(\boldsymbol{\theta})\ddot{\boldsymbol{\theta}} + C(\dot{\boldsymbol{\theta}}, \boldsymbol{\theta})\dot{\boldsymbol{\theta}} \tag{1}$$

where $\mathbf{n}$ is a 2×1 vector of shoulder and elbow joint torques, $I(\boldsymbol{\theta})$ is a 2×2 moment of inertia matrix, $C(\dot{\boldsymbol{\theta}}, \boldsymbol{\theta})$ is a 2×2 matrix specifying centrifugal and Coriolis effects, $\boldsymbol{\theta}$ is a 2×1 vector of shoulder and elbow joint angles, $\dot{\boldsymbol{\theta}}$ is a 2×1 vector of joint velocities and $\ddot{\boldsymbol{\theta}}$ is a 2×1 vector of joint accelerations. An explicit form of this expression can be found in Hollerbach and Flash (1982).

These resultant joint torques are generated by the three different groups of flexor and extensor single-joint elbow, single-joint shoulder and two-joint muscles (Fig. 3). Although muscle force is a complicated function of many variables, the dominant mechanical behavior may be represented by considering only the dependence on muscle length and its rate of change (Rack and Westbury 1969; Joyce et al. 1969). Hence in the interest of simplicity each of the above muscle groups was modelled as a linear spring in series with a viscous damping element (Hogan 1984). The resultant joint torques were assumed to depend only upon the instantaneous difference between the actual and equilibrium joint positions and upon joint velocities according to

$$\mathbf{n}(t) = R(t)(\boldsymbol{\phi}(t) - \boldsymbol{\theta}(t)) - B(t)\dot{\boldsymbol{\theta}}(t) \tag{2}$$

where $\boldsymbol{\theta} = (\theta_1(t),\ \theta_2(t))$ and $\phi = (\phi_1(t),\ \phi_2(t))$ are, respectively, the vectors of actual and equilibrium shoulder and elbow angles. The matrix R in (2) is the joint stiffness matrix at the equilibrium position

$$R = \begin{bmatrix} R_{11} & R_{12} \\ R_{21} & R_{22} \end{bmatrix}$$

and B is the joint viscosity matrix at the equilibrium position

$$B = \begin{bmatrix} B_{11} & B_{12} \\ B_{21} & B_{22} \end{bmatrix}.$$

The terms R_{11} and B_{11} in the above matrices are the net shoulder joint stiffness and viscosity, R_{12}, B_{12}, R_{21}, and B_{21} are the two-joint parameters and R_{22} and B_{22} describe the net elbow parameters.

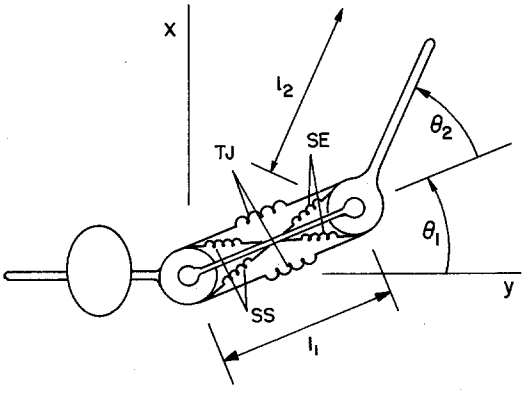

Fig. 3. A sketch of a planar two segment model of the upper limb and the spring-like muscles attached to it. *SS*, *SE*, and *TJ* represent, respectively, the single-joint shoulder, single-joint elbow and the two-joint muscles

4 The Simulator

Two types of computational modules diagrammed in Fig. 4 were developed in this study: *the equilibrium trajectory derivation* module and the *actual movement simulation* module. In the equilibrium trajectory derivation module, for measured time course of actual shoulder and elbow joint positions, velocities and accelerations, Eqs. (1) and (2) were solved explicitly to derive the time-histories of the equilibrium joint angles. The corresponding time courses of the equilibrium hand positions (x_e, y_e) were calculated from:

$$\begin{aligned} x_e &= l_1 \cos\phi_1 + l_2 \cos(\phi_1 + \phi_2) \\ y_e &= l_1 \sin\phi_1 + l_2 \sin(\phi_1 + \phi_2) \end{aligned} \tag{3}$$

where l_1 and l_2 are the lengths of upper segment of the arm and of the forearm, respectively.

The actual movement simulation module operated as follows: certain time-histories of the equilibrium joint angles were assumed and the values of the actual joint angles and velocities at the initial positions were

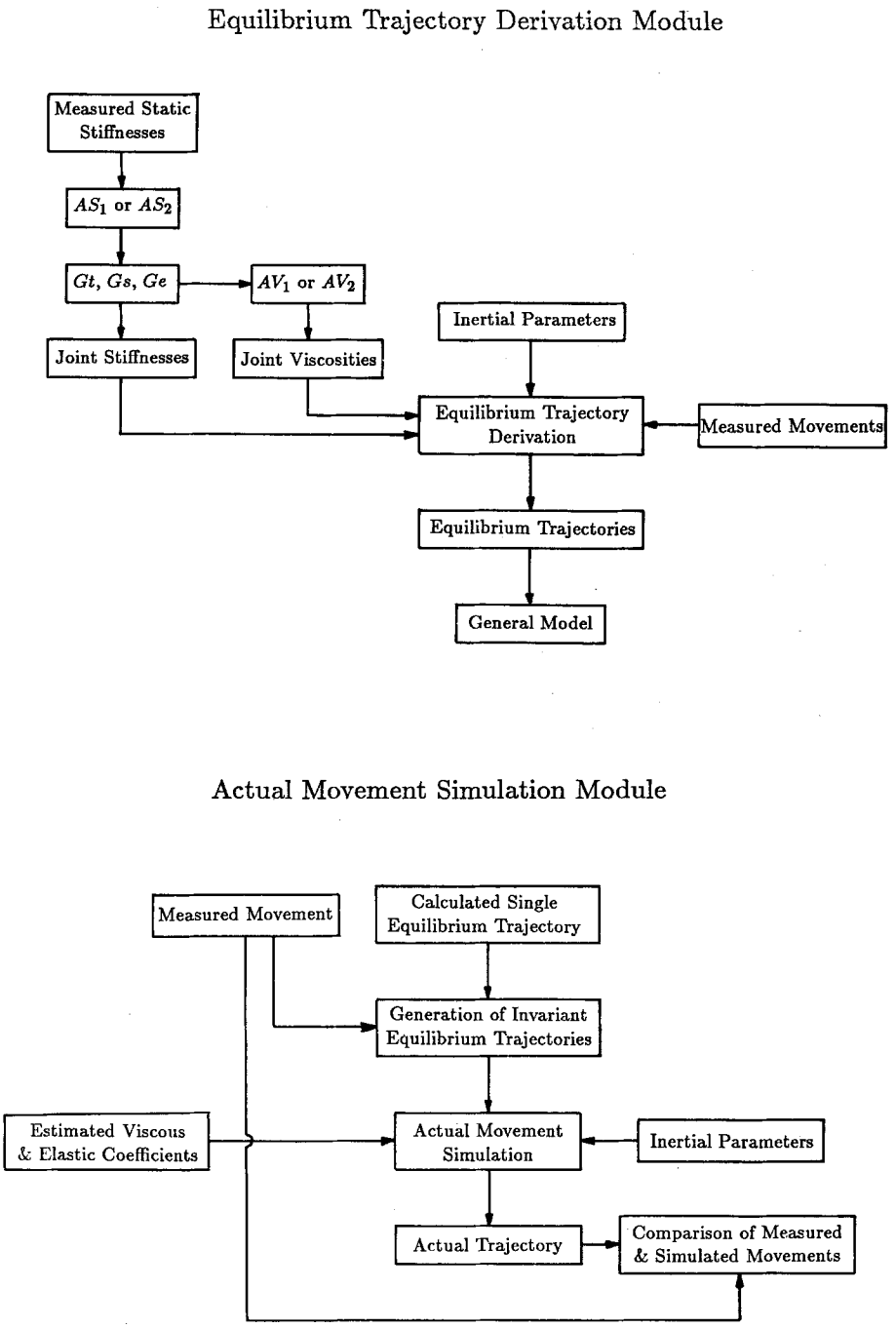

Fig. 4. Block diagram of the simulator

derived from measured movements. The resultant joint torques at the initial positions were calculated from (2) and substituted into (1) to derive the initial joint accelerations. Using numerical integration, the actual joint velocities and positions at the next instant were obtained. This procedure was repeated until the entire time-histories of the actual joint positions were derived. These predicted actual joint trajectories were then transformed into actual hand trajectories using (3).

As shown in Fig. 4, the values of three sets of parameters are needed in order to use these two types of computational modules: the arm geometric and inertial properties (link lengths, masses and inertias); the four elastic coefficients appearing in the joint stiffness matrix; and the four joint viscous coefficients. The inertial parameters of the forearm and upper arm segments for each subject, were derived from a computational model developed by Hatze (1979) using a battery of anthropomorphic measurements taken di-

rectly from the subject. Since the inertias and masses of the apparatus were one order of magnitude smaller than the typical masses and inertias of the human arm[1] the reaction forces generated by the apparatus were not taken into account in the simulations. To date, the values of the elastic and viscous coefficients during two-joint arm motions have not been measured. Because of this lack of experimental data the joint elastic coefficients used in this study were estimated from measured values of the corresponding static joint elastic coefficients.

4.1 Estimation of Joint Elastic and Viscous Coefficients

4.1.1 Elastic Coefficients. It is conceivable that neural and anatomical constraints limit the ability of the system to modify the stiffness ellipse (Flash and Mussa-Ivaldi 1984). These factors are also present during movement. Consequently, it is postulated here that the shape and orientation of the stiffness field when the hand moves through any workspace location are similar to the ones observed for the static field at that location. One should bear in mind, however, that the size parameter of the static stiffness field was found to increase following the application of disturbance forces, and even in the absence of such forces the size parameter did vary among subjects and over time. Since muscle stiffness increases with muscle force and level of activation (Hoffer and Andreassen 1981; Cannon and Zahalak 1982), and given the higher levels of muscle activation during movement, in our movement simulations we did introduce the possibility for increasing the size of the stiffness field compared to its size during posture. To derive the joint elastic coefficients used in this study, the hand stiffness matrices were measured at 15 hand positions and transformed into the corresponding joint stiffness matrices. The joint elastic coefficients R_{11}, R_{12}, and R_{22} which were used in both computational modules were estimated from the corresponding measured static coefficients, based on one of two alternative sets of assumptions, AS_1 and AS_2 (see Fig. 4).

AS_1: The elastic coefficients selected according to this set of assumptions are only rough estimates of the corresponding static joint elastic coefficients. Since the values of all three static joint stiffnesses (derived from the symmetric hand stiffness matrices) did not vary extensively with hand position, in AS_1 it was assumed that the values of R_{11}, R_{12}, and R_{22} remain constant throughout the workspace. Each one of these constant joint elastic coefficients was obtained from the average value of the 15 measured values of the corresponding static joint elastic coefficient.

AS_2: Under AS_2 the estimated joint stiffnesses were determined according to the local values of the corresponding static stiffnesses. Consequently, the values of the joint elastic coefficients were repeatedly updated according to the instantaneous values of the shoulder and elbow joint angles. At the positions where direct measurements of the four elements of the joint stiffness matrix were not available, they were computed using a third order least square interpolation.

4.1.2 Scaling of Joint Stiffnesses. Under the assumption that the stiffnesses might be higher in motion than in posture, the values of the elastic coefficients estimated according to either AS_1 or AS_2 were multiplied by constant scaling factors ranging between 1.0 and 3.0. The values of these scaling factors were selected based on the following analysis. The symmetric joint stiffness matrices appearing in (2) can also be written as

$$R=\begin{bmatrix} R_s+R_t & R_t \\ R_t & R_e+R_t \end{bmatrix}.$$

As shown in the Appendix, if the lengths of the forearm and upper arm are equal (which is roughly the case for the human arm), and if $R_{11}=2R_{12}$ (or accordingly, if $R_s=R_t$), the major axis of the hand stiffness field is directed along the radial axis of a polar coordinate system whose origin is located at the shoulder. In this case the expression for the shape of the stiffness ellipse is

$$\frac{S_{rr}}{S_{\phi\phi}}=\left(1+\frac{2R_e}{R_t}\right)\cot^2\theta_2/2 \tag{4}$$

where S_{rr} and $S_{\phi\phi}$ are the stiffnesses in the radial and polar directions, respectively. It was confirmed by Flash and Mussa-Ivaldi (1984) that at most hand locations R_{11} approximately equals $2R_{12}$. This explains why the orientation of the hand stiffness ellipse was found to be roughly polar throughout the workspace.

In the simulations presented here the values of R_t, R_s, and R_e were first calculated from R_{11}, R_{12}, and R_{22} and the resulting values were then multiplied by the constant gain factors G_t, G_s, and G_e, respectively. As can be seen from (4), for a polar stiffness field if $G_s=G_t\neq G_e$, only the shape parameter changes. If $G_t=G_s=G_e$ only the size of the stiffness ellipse changes. A change only in the orientation of the stiffness ellipse can be achieved by rotating the entire hand stiffness

[1] The mass of the proximal link of the apparatus was 298 g and its length was 28 cm. The mass of the distal link of the apparatus was 156 g and its length was 43.5 cm

matrix. In the simulations presented here the values of G_e, G_s, and G_t were chosen so as to preserve, as much as possible, the local values of the orientation of the static stiffness ellipse while allowing for its size to be changed. In attempting to get the best possible match between the measured and simulated actual movements we did introduce, however, slight modifications especially in the shape of the static stiffness field. The elastic coefficients R_{11}, R_{12}, and R_{22} which were used in the simulations were then obtained from: $R_{11}=G_tR_t+G_sR_s$, $R_{12}=G_tR_t$, and $R_{22}=G_tR_t+G_eR_e$.

4.1.3 Viscous Coefficients. To date no measurements of joint viscosities during two-joint arm movements have been performed. However, single-joint viscosities were measured and were found to increase with the levels of muscle activation (Cannon and Zahalak 1982; Lacquaniti et al. 1982) and to change with joint angle (MacKay et al. 1986). According to Cannon and Zahalak (1982) the ratio between joint viscosity and stiffness (τ) is nearly constant for muscle torques ranging between 3.0 to 30.0 N-m. The mean values of the measured τ were found to be 0.045 s for the flexors and 0.05 s for the extensors. Lacquaniti et al. (1982) found that when the task involved the active resistance to small pseudo-random perturbations, both elbow stiffness and viscosity increased relatively to their values in the passive task, the increment in stiffness being larger than in viscosity. In the transition from the "do not resist" to the "resist" tasks, the mean value of τ decreased frem 0.08 s in the passive task to 0.025 s in the "resist" task while the mean value of the damping ratio $\varrho=\sqrt{B^2/4KI}$ (I is the forearm inertia), decreased from 0.338 to 0.218. In the opposite transition the mean value of ϱ changed very slightly from 0.448 in the "resist" task to 0.476 in the "do not resist" task while the mean value of τ increased from 0.058 to 0.125 s. Based on the above experimental data it is impossible to unequivocally determine what the relationship between joint viscosity and stiffness is. Thus, in the simulation work presented here joint viscosities were derived from joint stiffnesses according to one of two alternative assumptions AV_1 and AV_2 (see Fig. 4).

AV_1: Under this assumption B_{11}, B_{12}, and B_{22} were derived from $B_{ij}=\tau R_{ij}$. The values of τ were chosen to be in the range between 0.05 s and 0.125 s and the same value of τ was used for all three viscous coefficients.

AV_2: Under this assumption $B_{ij}=2\varrho\sqrt{I_{ij}R_{ij}}$. The same damping ratio was used for all three viscous coefficients (I_{ij} is the i,j element of the inertia matrix). The value of ϱ was chosen in the range between 0.35 and 1.5.

5 Results

5.1 Derivation of Equilibrium Trajectories

By applying the equilibrium trajectories derivation module, hand equilibrium trajectories were first derived from several measured movements under the combination of AS_1 and AV_1 each time using a different set of values for G_t, G_s, G_e, and τ. The values of these parameters were kept constant throughout the entire duration of the movement. For $G_t=G_s=G_e=1.0$ and $\tau=0.05$ s the equilibrium hand positions were found to be very close to the measured positions but for $G_t=G_s=G_e=1.0$ and $\tau=0.1$ s the equilibrium trajectories were found to be straighter than the measured actual trajectories. The three scaling factors, G_s, G_t, and G_e were then picked so as to preserve the orientation and shape of the static ellipse but to allow its size to increase. Representative results from this procedure are illustrated in Fig. 5A. These results were obtained using the following values: $R_{11}=29.5$, $R_{12}=14.3$, $R_{22}=39.3$ N-m/rad, $G_t=2.0$, $G_s=2.0$, $G_e=2.0$, and $\tau=0.1$ s. As these plots indicate, the calculated hand equilibrium trajectories follow straighter paths than the ones generated by our subjects. Since, in principle, the equilibrium trajectories could have been found to follow any one of a large number of possible paths, this was a surprising finding and one which was not expected a priori.

We then derived hand equilibrium trajectories from measured movements directed along the radial direction passing through the shoulder. This time the equilibrium trajectories were directed under the combination of AS_2 and AV_2 using each time a different set of values for G_t, G_s, G_e, and ϱ. By preserving the orientation of the static stiffness field, and slightly modifying its shape, increasing its size, and picking an appropriate value for ϱ, the equilibrium trajectory shown in Fig. 5B could be derived. Comparisons between the time course of the equilibrium and actual positions along y axis are shown in Fig. 5C. The speed profiles of the equilibrium and actual trajectories are shown in Fig. 5D. As this figure indicates the resulting hand equilibrium trajectory follows a straight hand path between the movement end-points. The geometric parameters (size, shape and orientation) of the static hand stiffness ellipse at the initial position were, respectively, 20.9, 12.18, and 90.75°. The corresponding values of of the hand stiffness ellipse used to generate this equilibrium trajectory at the initial position were, respectively, 138.05, 8.96, and 90.61°.

5.2 The Form of Hand Equilibrium Trajectories: A General Hypothesis

The results presented in the previous section as well as the reported qualitative similarities between measured

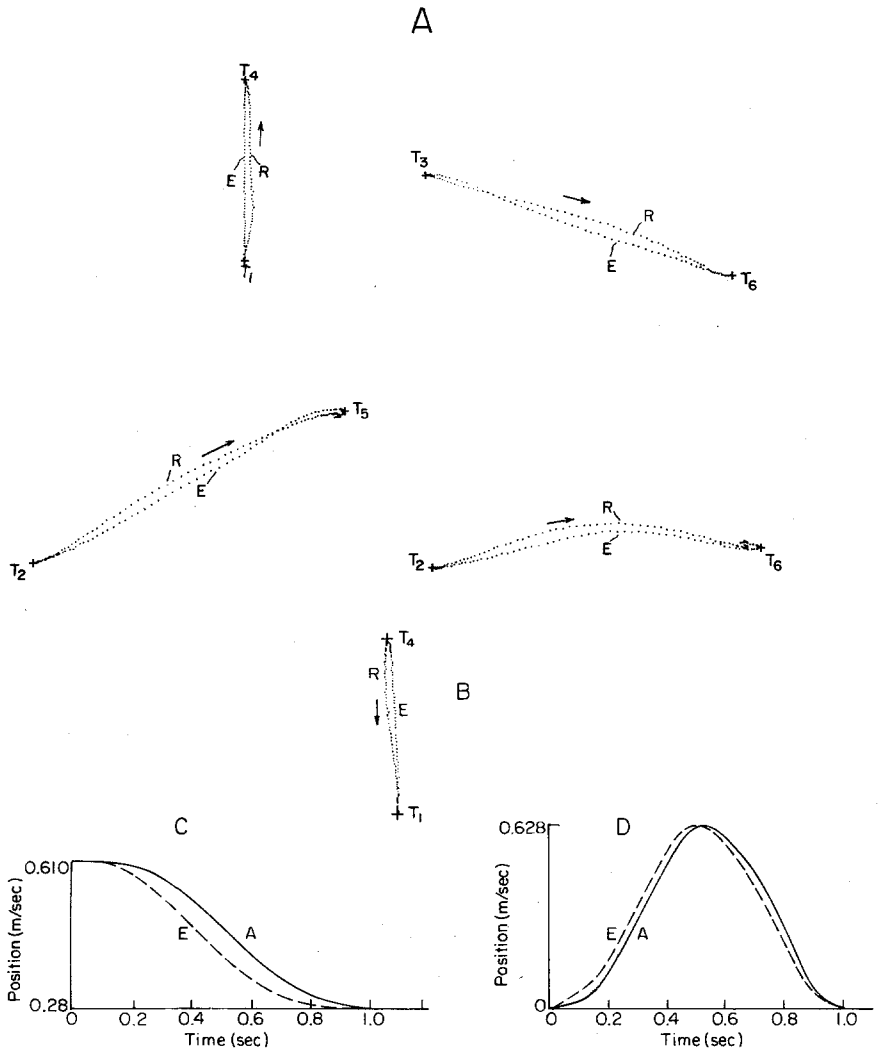

Fig. 5A–D. Typical equilibrium trajectories derived from measured movements. **A** Hand equilibrium paths (E) derived from measured movements (R) under the combination of AS_1 and AV_1. **B** A hand equilibrium path (E) derived from a measured radial movement (R) under the combination of AS_2 and AV_2. The static joint stiffnesses at the initial position were: $R_{11}=32.64$, $R_{12}=17.32$, and $R_{22}=26.48$ N-m/rad. $G_s=3.0$, $G_t=3.0$, $G_e=1.5$, and $\varrho=0.35$. **C** The y-coordinates of the hand equilibrium (dashed line) and actual (solid line) positions for the trajectories in 5B. **D** Speed profiles of the equilibrium (dashed line) and radial (solid line) trajectories shown in Fig. B

movements performed in different parts of the workspace (especially the straightness of the measured hand paths) were suggestive of a much more general hypothesis, namely, that all unconstrained point-to-point reaching movements are generated by specifying neural control signals required to shift the hand equilibrium position along straight lines connecting the movement end-points (Fig. 6). Hence it is assumed that all hand equilibrium trajectories can be mathematically described by the following expression

$$\mathbf{r}_e(t)=\mathbf{r}_i+\mathbf{a}f(t) \tag{5}$$

where $\mathbf{r}_e(t)=(x_e(t), y_e(t))$ describes the equilibrium position coordinates of the hand at time t, $\mathbf{r}_i=(x_i, y_i)$ is the location of the hand at $t=0$ and $\mathbf{a}=(x_f-x_i, y_f-y_i)$ is the movement amplitude where (x_f, y_f) is the final hand position. It is also suggested here that the rate according to which the equilibrium position is shifted dictates the speed of the actual movement. Based on the observed motor behavior, it is postulated that the shape of the speed profile of the hand equilibrium trajectory is the same for all reaching movements. The function $f(t)$ is therefore assumed to be invariant under translation, rotation, time, and amplitude scaling.

In principle, we could have derived several equilibrium trajectories from several measured movements, and test whether they all have a similar form which can be described by (5). Instead, we preferred to produce actual movements based on the use of a single calculated equilibrium trajectory and to test whether these simulated movements capture the kinematic features of the corresponding measured movements. For this purpose, for each subject we derived a hand equilibrium trajectory from a measured movement along the radial direction passing through the shoulder (see Fig. 5B) and applied it to other parts of the workspace. Seeing that this equilibrium trajectory followed a straight path, we substituted the coordi-

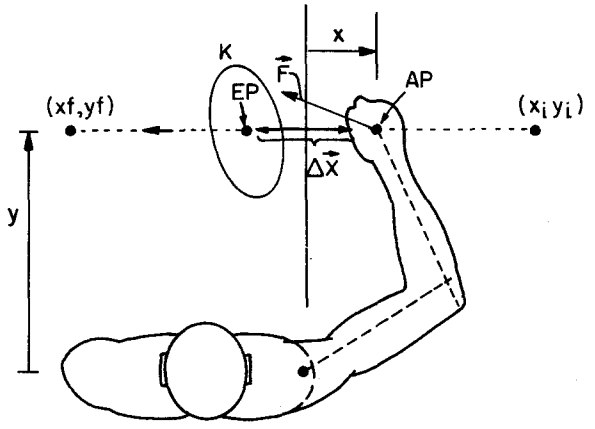

Fig. 6. A graphical representation of the *equilibrium trajectory control hypothesis*. *Ap* and *Ep* are, respectively, the actual and equilibrium positions of the hand. $\Delta\mathbf{x}$ is the displacement vector from equilibrium, *K* is the hand stiffness ellipse about the equilibrium position and **F** is the restoring force vector acting on the hand. The points (x_i, y_i) and (x_f, y_f) are the initial and final hand positions. The dashed line represents the equilibrium trajectory path

nates of the movement end-points in (5), and calculated the time course $f(t)$, which was then normalized for a movement duration of 1000 ms. To generate a hypothetical equilibrium trajectory between any other pair of targets, the coordinates of these targets and the computed time course of the normalized $f(t)$ were again substituted into (5) and the resulting equilibrium trajectory was scaled according to the desired duration of movement.

5.3 *Simulated Actual Movements*

In this section we present actual hand trajectories which were produced based on the hypothetical equilibrium trajectories. The actual trajectories were first simulated, employing AS_2 and AV_2 and using a series of values for G_t, G_s, G_e, and ϱ (actual movements simulated under the combination of AS_2 and AV_1 will be presented below in Sect. 5.4). For a wide range of values of these parameters, and even in the case that $G_t = G_s = G_e = 1.0$, the simulated hand paths deviated from the straight equilibrium hand paths in the same direction as the measured movements. Nevertheless good agreement between the exact values of the measured and predicted actual hand positions could be achived for particular values of these parameters.

In Figs. 7 and 8 several simulated hand trajectories are compared with the corresponding measured trajectories. The values of the different parameters used to simulate the movements shown in Figs 7 and 8 are given in Tables 1 and 2, respectively. Also compared in these tables are the geometrical parameters of the static and assumed dynamic stiffness ellipses at the initial positions. Notice in Figs. 7 and 8 the excellent fit between the predicted and measured trajectories and the success of the simulations in capturing the kinematic features of the measured movements down to fine

Table 1. Values of the different parameters used in the simulations of movements 1–4 shown in Fig. 7 and a comparison between the geometrical parameters of the static and estimated dynamic hand stiffness ellipses at the initial positions

Movement	Static joint stiffnesses $nw \times$ m/rad	Scaling factors and damping coefficient	Dynamic joint stiffnesses $nw \times$ m/rad	Joint viscosities $nw \times m \times$ s/rad	Geometrical parameters: static stiffness ellipses	Geometrical parameters: dynamic stiffness ellipses
1 (subject 1)	$R_{11}=20.10$ $R_{12}=8.33$ $R_{22}=37.83$	$G_s=3.0$ $G_t=3.0$ $G_e=2.0$ $\varrho=0.4$	$R_{11}=85.29$ $R_{12}=24.99$ $R_{22}=83.99$	$B_{11}=3.75$ $B_{12}=0.48$ $B_{22}=1.764°$	Shape=1.63 Size=22.1 Orientation =100.55°	Shape=1.35 Size=141.9 Orientation =121.46°
2 (subject 1)	$R_{11}=32.73$ $R_{12}=17.73$ $R_{22}=40.52$	$G_s=1.5$ $G_t=2.25$ $G_e=1.0$ $\varrho=0.35$	$R_{11}=62.1$ $R_{12}=39.0$ $R_{22}=62.2$	$B_{11}=3.34$ $B_{12}=1.30$ $B_{22}=1.49$	Shape=5.60 Size=19.91 Orientation =100.02°	Shape=3.69 Size=46.21 Orientation =105.01°
3 (subject 1)	$R_{11}=32.8$ $R_{12}=17.4$ $R_{22}=46.76$	$G_s=1.5$ $G_t=1.5$ $G_e=2.5$ $\varrho=0.5$	$R_{11}=49.2$ $R_{12}=26.1$ $R_{22}=89.5$	$B_{11}=3.63$ $B_{12}=1.00$ $B_{22}=2.56$	Shape=1.75 Size=24.06 Orientation =132.81°	Shape=2.68 Size=81.75 Orientation =133.50°
4 (subject 1)	$R_{11}=32.86$ $R_{12}=17.16$ $R_{22}=43.16$	$G_s=2.5$ $G_t=2.5$ $G_e=1.0$ $\varrho=0.8$	$R_{11}=80.7$ $R_{12}=42.9$ $R_{22}=68.9$	$B_{11}=7.25$ $B_{12}=1.95$ $B_{22}=3.55$	Shape=1.75 Size=25.46 Orientation =131.36°	Shape=1.07 Size=84.27 Orientation =171.5°

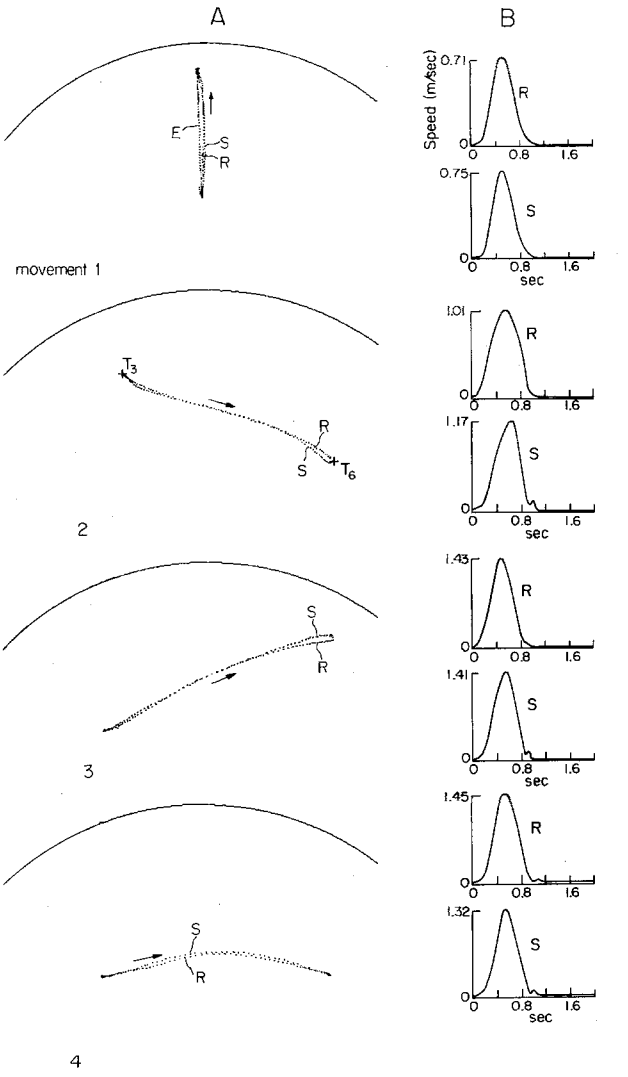

Fig. 7A and B. Comparisons between measured (R) and simulated (S) hand trajectories derived under the combination of AS_2 and AV_2. **A** Hand paths. **B** Speed profiles. E represents the equilibrium trajectory. The values of the different parameters used to derive these simulated trajectories are shown in Table 1

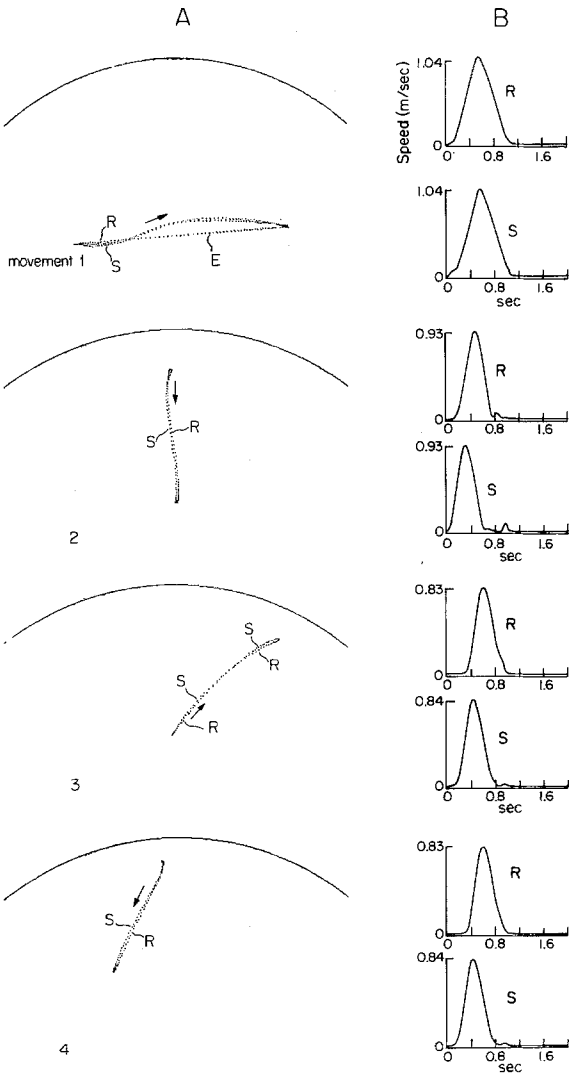

Fig. 8. See Fig. 7 for legend description. The values of the different parameters used to derive the simulated trajectories are shown in Table 2

details of curvature. Notice also the little hooks in the predicted trajectories, when the hand approaches the target. The values presented in Tables 1 and 2 indicate that the size parameters of the assumed dynamic hand stiffness matrices are higher than the corresponding values of the hand static stiffness ellipses. The orientation parameters are not significantly different from those of the corresponding static stiffness matrices (except for movement 4 in Fig. 7). The modifications introduced in the shapes of the static stiffness ellipses are also within the range of changes that occur following the application of disturbance forces.

5.3.1 Changing Movement Direction. Figure 9A and 9C show several hand paths for movements in two opposite directions between two different pairs of targets recorded from one subject. In Fig. 9B and 9D predicted trajectories between the same target pairs and for both movement directions are compared to measured movements obtained during single trials. Although all equilibrium trajectories are assumed to follow straight paths regardless of movement direction, for movements in opposite directions the predicted as well as the measured trajectories display different patterns of deviations from straight paths. The reason for this behavior will be explained in the discussion.

5.3.2 Changing Movement Speed. It has been shown that the scaling of actual trajectories with speed, i.e.

Table 2. Movements 1–4 in Fig. 8: see Table 2 for legend description

Movement	Static joint stiffnesses $nw \times$ m/rad	Scaling factors and damping coefficient	Dynamic joint stiffnesses $nw \times$ m/rad	Joint viscosities $nw \times m \times$ s/rad	Geometrical parameters: static stiffness ellipses	Geometrical parameters: dynamic stiffness ellipses
1 (subject 2)	$R_{11}=34.86$ $R_{12}=18.20$ $R_{22}=45.40$	$G_s=1.5$ $G_t=1.5$ $G_e=2.0$ $\varrho=0.7$	$R_{11}=52.20$ $R_{12}=27.30$ $R_{22}=81.9$	$B_{11}=8.17$ $B_{12}=4.18$ $B_{22}=7.24$	Shape=1.45 Size=30.7 Orientation =144.95°	Shape=1.81 Size=86.62 Orientation =142.66°
2 (subject 2)	$R_{11}=32.43$ $R_{12}=17.23$ $R_{22}=26.8$	$G_s=3.0$ $G_t=3.0$ $G_e=1.5$ $\varrho=0.35$	$R_{11}=97.1$ $R_{12}=51.7$ $R_{22}=66.1$	$B_{11}=4.65$ $B_{12}=1.82$ $B_{22}=2.13$	Shape=6.47 Size=15.48 Orientation =91.62°	Shape=4.72 Size=101.68 Orientation =91.65°
3 (subject 3)	$R_{11}=20.3$ $R_{12}=8.5$ $R_{22}=36.90$	$G_s=1.5$ $G_t=1.0$ $G_e=2.7$ $\varrho=0.7$	$R_{11}=26.2$ $R_{12}=8.5$ $R_{22}=85.2$	$B_{11}=3.44$ $B_{12}=0.54$ $B_{22}=3.30$	Shape=2.03 Size=20.40 Orientation =107.84°	Shape=3.81 Size=65.12 Orientation =102.00°
4 (subject 3)	$R_{11}=30.13$ $R_{12}=16.33$ $R_{22}=41.33$	$G_s=3.0$ $G_t=3.0$ $G_e=1.5$ $\varrho=0.7$	$R_{11}=90.5$ $R_{12}=49.0$ $R_{22}=86.5$	$B_{11}=4.93$ $B_{12}=1.33$ $B_{22}=2.37$	Shape=2.12 Size=22.78 Orientation =120.33°	Shape=1.31 Size=126.34 Orientation =126.58°

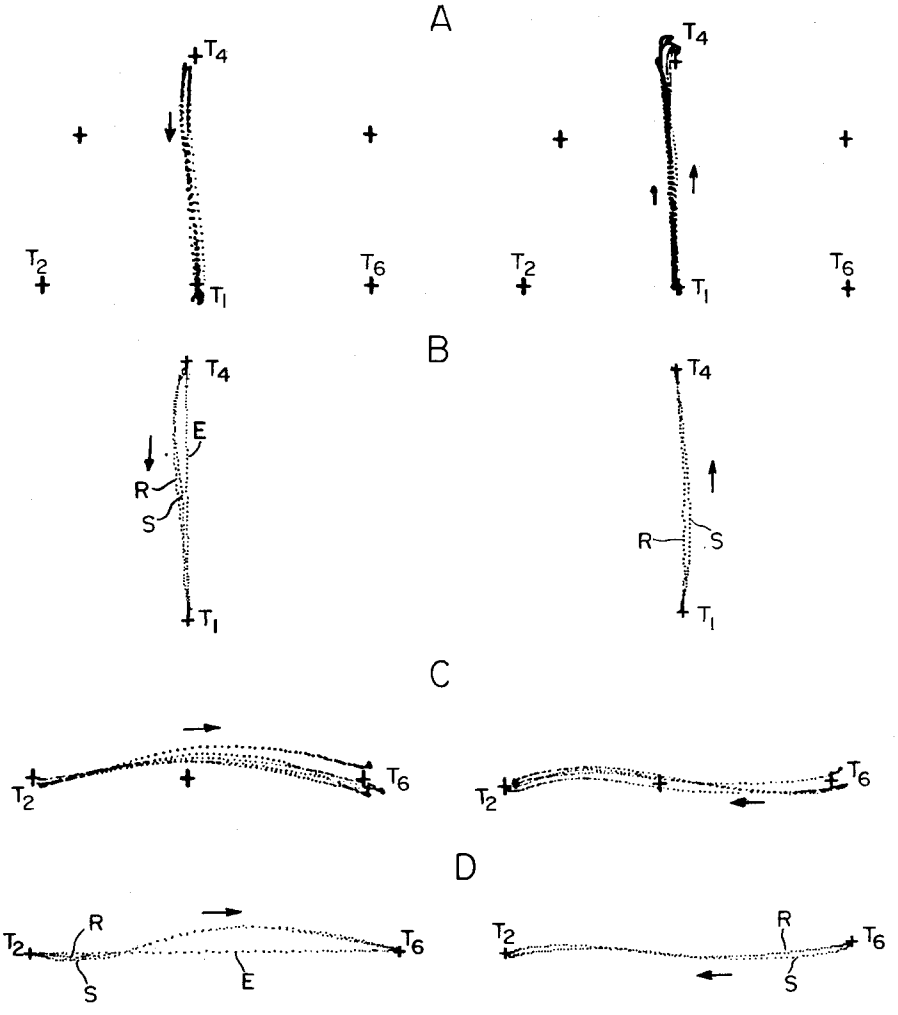

Fig. 9. **A** Hand paths for several measured movements in opposite directions between T_1 and T_4 recorded from one subject. **B** Comparisons between simulated (S) and single-trial measured (R) movements between T_1 and T_4 for both movement directions. For the movement from T_1 to T_4, $G_t=3.0$, $G_s=3.0$, $G_e=2.0$, $\varrho=0.4$. For the movement from T_4 to T_1, $G_t=3.0$, $G_s=3.0$, $G_e=1.5$, $\varrho=0.35$. **C** Hand paths for several measured movements in opposite directions between T_2 and T_6. **D** Comparisons between simulated (S) and single-trial measured (R) movements between T_2 and T_6 for both movement directions. For the movement from T_2 to T_6, $G_t=2.0$, $G_s=2.0$, $G_e=3.5$, $\varrho=0.8$. For the movement from T_6 to T_2, $G_t=2.5$, $G_s=2.5$, $G_e=2.0$, $\varrho=0.7$

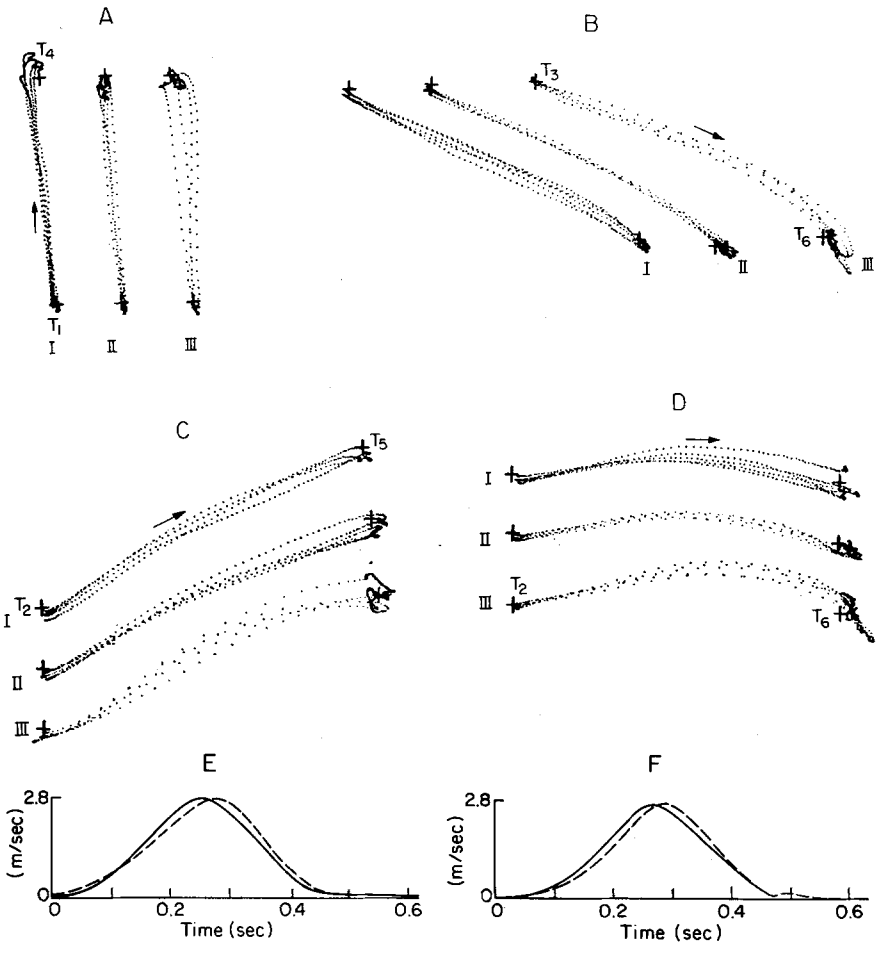

Fig. 10A–F. I: measured hand paths for movements lasting more than 0.8 s. II: measured hand paths for movements lasting between 0.5 and 0.8 s. III: measured hand paths for movements lasting between 0.4 and 0.5 s. **A** Movements from T_1 to T_4. **B** Movements from T_3 to T_6. **C** Movements from T_2 to T_5. **D** Movements from T_2 to T_6. **E** Overlapped speed profiles from fast (solid line) and slow (dashed line) movements between T_2 and T_5. **F** The same as in **E** for fast and slow movements between T_2 and T_6

$(\dot{\theta}'_1(t), \dot{\theta}'_2(t)) = s(\dot{\theta}_1(st), \dot{\theta}_2(st))$, implies that joint torques also must be scaled by a constant factor equal to s^2, where $s>1$ is the ratio between the movement durations for the slow and fast movements (Hollerbach and Flash 1982). It is assumed in this work that the speed of the hand equilibrium trajectories is scaled by the same factor s, i.e. $(\dot{\phi}'_1(t), \dot{\phi}'_2(t)) = s(\dot{\phi}_1(st), \dot{\phi}_2(st))$. This implies that to generate faster movements, the system must also generate higher joint stiffnesses and viscosities so that $R'_{ij}(t) = s^2 R_{ij}(st)$ and $B'_{ij}(t) = sB_{ij}(st)$, where $R_{ij}(st)$ and $B_{ij}(st)$ are the joint stiffnesses and viscosities for the slower movements.

Variations in the measured hand paths with movement speed are illustrated in Fig. 10A–D, where data are presented for several movements recorded from one of the subjects. Notice that for movements lasting between 0.5 and 0.8 s (sets II), the hand follows very similar paths to those followed during slower movements (sets I). Only for movements lasting less than 0.5 s (sets III) do the hand paths differ from the ones shown in sets I and II. To examine whether measured actual trajectories do indeed scale uniformly with speed for all achievable movement speeds, hand speed profiles for slower movements were uniformly scaled and superimposed on the appropriate profiles of measured fast movements. This analysis indicated that for movements lasting more than 0.5 s, trajectories indeed scale uniformly with speed. Only at very high speeds (Fig. 10E and 10F), the velocity profiles do not scale uniformly, and are more skewed towards the left. Notice that the measured trajectories at these speeds display increased oscillatory behavior and larger overshoots when the hand approaches the target.

It is possible that at very high speeds, the required magnitudes of the appropriately scaled stiffnesses and viscosities exceed the maximal magnitudes which the system is capable of generating. The hypothesis that the system may manage to generate only smaller stiffnesses and viscosities than those required was tested. As indicated by Fig. 11, a simulated movement between T_3 and T_6 with 0.4 s duration could be made to match the real movement when the joint stiffnesses and viscosities used in the simulation of the corresponding 1.0 s movement, were scaled by 2.5. For the movement between T_1 and T_4, however, good agreement between the predicted and measured movements was only

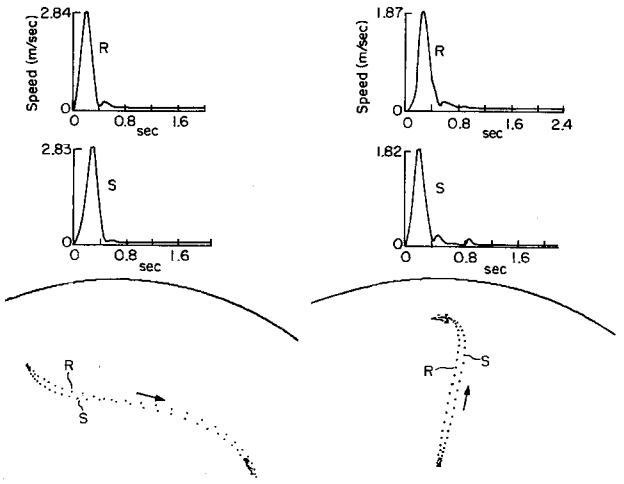

Fig. 11. Comparisons between simulated (S) and measured (R) 0.4 s trajectories. Upper part of figure: speed profiles. Lower half: hand paths. For the movement from T_3 to T_6, $G_t=5.625$, $G_s=3.75$, $G_e=2.5$, $\varrho=0.55$. For the movement from T_1 to T_4, $G_t=3.5$, $G_s=5.0$, $G_e=1.0$, $\varrho=0.5$

achieved when considerable modifications in the shape and orientation of the stiffness and viscosity fields were introduced.

5.4 *Sensitivity Analysis*

In this section we will show how the reference simulated trajectories (those shown in Figs. 7 and 8) change when we introduce changes either in the joint stiffness and viscosity matrices, in the stiffness-viscosity relationship, or in the time profiles of equilibrium trajectories. For each modification in model parameters the new simulated trajectory will be shown together with the corresponding measured movement. The effects of increasing the size of the stiffness and viscosity ellipses while preserving their shape and orientation resulted in hand paths which deviated less from the straight paths connecting the movement endpoints than the measured trajectories (Fig. 12A). Hand paths resulting from changes in the shape of the stiffness and viscosity ellipses are shown in Fig. 12B and 12C. In Fig. 12B the hand was made stiffer in the radial direction, while in Fig. 12C the the stiffness field was made stiffer in the polar direction. As can be seen from both figures, these modifications resulted in greater position discrepancies between the simulated and the measured hand paths than those obtained for the simulated reference paths. However, the changes did not introduce qualitatively significant changes in the curvatures of the simulated movements. When the two-joint stiffnesses were assumed to be 0.0 (Fig. 12D) the deviations of the simulated hand paths from the measured trajectories were larger than the ones obtained for the reference paths and their magnitudes depended on the workspace region.

As shown in Fig. 13A when the alternative stiffness-viscosity relationship $B_{ij}=0.1\,R_{ij}$ (AV_1) was used the resulting hand paths deviated less from straight lines than both the measured and reference paths. Among the four different elements of the inertia matrix the values of the elements I_{11} and I_{12} depend on $\cos\theta_2$. Hence under AV_2, the values of B_{11} and B_{12} also depend on $\cos\theta_2$. We repeated the simulations, this time eliminating the dependency of joint viscosities on elbow angles by assuming that $B_{ij}=2\varrho\sqrt{I_{ij}(0)K_{ij}}(I_{ij}(0)$

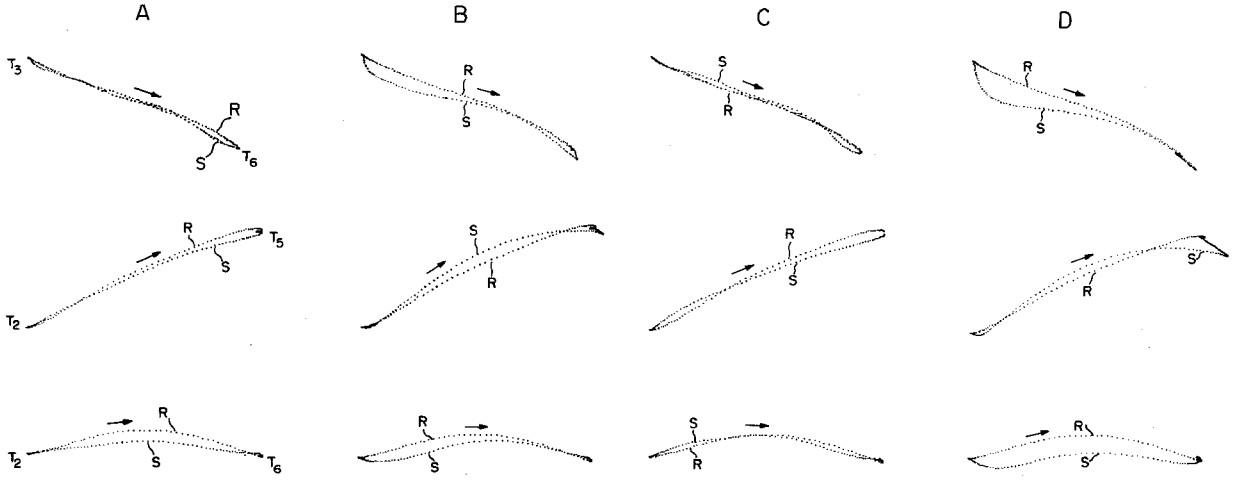

Fig. 12. **A** Increasing the size of the stiffness and viscosity ellipses while preserving their shape and orientation (all joint stiffnesses were multiplied by $c=2$). **B** Changes in the shape of the stiffness and viscosity ellipses: the single-joint elbow stiffnesses were multiplied by $\sqrt{3}$ and the two-joint and single-joint shoulder stiffnesses were divided by $\sqrt{3}$. **C** Changes in the shape of the stiffness and viscosity ellipses: the stiffness field was made stiffer in the polar direction ($c=1/\sqrt{3}$). **D** The two-joint stiffnesses were assumed to be 0.0

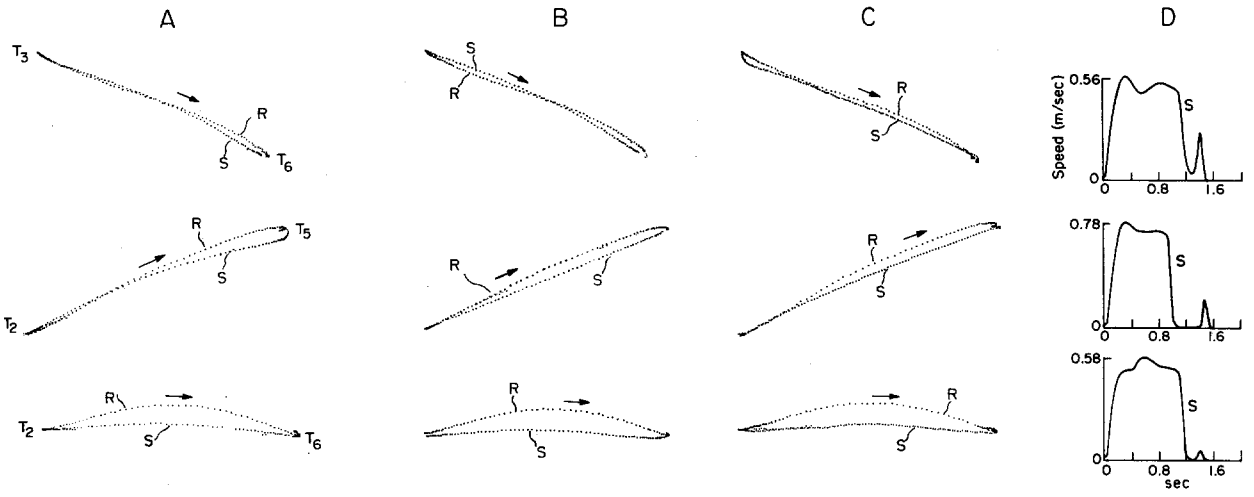

Fig. 13. **A** Simulated hand paths resulting from the use of the alternative stiffness-viscosity relationship $B_{ij}=0.1\,R_{ij}$. **B** Simulated hand paths (*S*) resulting from the use of a constant hand stiffness matrix with zero off-diagonal terms. The viscosities were chosen so that $B_{ij}=0.1\,R_{ij}$. **C** Simulated hand paths (*S*) obtained from equilibrium trajectories with straight hand paths and constant speeds of motion. **D** Hand speed profiles for the simulated movements shown in **C**

is the value of the i,j element of the inertia at $t=0$). The resulting simulated actual trajectories (not shown here) were found to be indistinguishable from the reference simulated trajectories. Figure 13B shows simulated hand paths derived when the hand stiffness matrix in Cartesian coordinates is assumed to stay constant throughout the entire movement and to have zero off-diagonal elements (joint viscosities were chosen under AV_1). These simulated hand paths again deviate less from the straight paths than the measured ones. The equilibrium trajectories normally used in the simulations had unimodal speed profiles (see Fig. 5). Figure 13C shows the predicted hand paths and speed profiles resulting from equilibrium trajectories with straight hand paths and constant speeds of motion of the equilibrium point. Such equilibrium trajectories result in straighter hand paths than those observed for the measured movements and the hand speed profiles of the simulated trajectories are also shown to be unrealistic (Fig. 13D).

6 Discussion

Based on the kinematic characteristics of the calculated hand equilibrium trajectories, and given the tendency of all measured movements to have similar qualitative features, we postulated that the hand equilibrium trajectories underlying reaching movements may all have the same form. This hypothesis was tested by investigating whether the hypothetical hand equilibrium trajectories can give rise to actual movements that match those generated by our subjects. The kinematic features of the predicted trajectories agreed with those of the measured movements including kinematic details such as the wiggling of hand trajectories and their characteristic deviations from straight paths depending on the workspace region within which the movement was generated and on the direction of motion. The model also predicted the existence of overshoots in the path when the hand approaches the target, in cases when the stiffness and viscosity parameters did not provide adequate damping.

Two factors may give rise to the observed differences between the curvatures of different simulated movements. First, for movements along different straight line paths the torque profiles are quite different (Hollerbach and Flash 1982). For example, during reaching movements which involve rotations of the shoulder and elbow joints in opposite directions (e.g. movements in the radial directions), the velocity (centripetal and Coriolis) torques have diminished influence as compared to whipping movements (e.g. movents across the body). During reaching movements the shoulder and elbow inertial torques cancel each other out, but work together during whipping movements. Second, the degree by which the shape and orientation of the hand stiffness field change along the straight line path is also quite different. Together, these effects tend to cause smaller deviations of the hand from the straight equilibrium paths in the case of radial movements, for example, as compared to movements across the body. Given the success of the model in accounting for the fine details of movement curvature, it can be argued that trajectory deviations seen in real movements also result from similar interactions between visco-elastic and inertial effects. As was shown

by the sensitivity analysis, the nature of the speed profile of the equilibrium trajectory may also influence the degree to which the hand deviates from the straight line path of the equilibrium trajectory.

The differences between the curvature of movements performed between the same pair of targets but in opposite directions, also result from the interactions between inertial and visco-elastic effects. If the kinematic trajectory plan specifies the same kind of hand trajectory for movements in opposite directions, the magnitudes and signs of the required elbow and shoulder joint torques will be the same at any particular location along the path regardless of the direction of motion (see Fig. 14A). To assess the causes for the differences between trajectory deviations of movements in opposite directions, consider the following expression for the initial hand acceleration:

$$\ddot{\mathbf{x}}(0) = M(0)\,K(0)\,(\mathbf{x}_e(0) - \mathbf{x}(0)) \qquad (7)$$

where $K(0)$, $M(0)$, and $(\mathbf{x}_e(0) - \mathbf{x}(0))$ are, respectively, the initial hand stiffness and mobility (inverse of inertia) matrices in workspace coordinates, and the initial displacement vector of the hand from the equilibrium point. Since, in general, MK is not proportional to the identity matrix, the initial hand direction will not be directed along the desired straight line. Moreover, as shown in Fig. 14B, those components of the initial acceleration which tend to make the hand deviate away from the straight path, point in opposite directions for the two opposing movements.

To obtain numerical predictions of equilibrium and actual trajectories, a linear model of the neuromuscular system was assumed. This is obviously a simplification. For example, Gielen and Houk (1984) have shown that viscosity does depend on velocity. In the model presented here, the dynamics of muscle excitation-contraction coupling and the time-histories of agonist/antagonist activations (Hallett and Marsden 1979) were also ignored. Had these factors been included in the model, it is possible that equilibrium trajectories with more uniform speed profiles would have been obtained. However, it has been shown by Hogan (1984) that the gradual transition of the equilibrium position observed during elbow movements is not merely a consequence of the sluggish response of muscle to an abrupt change in the neural input. In addition, according to Atkeson and Saund (1984) the magnitudes of elbow stiffnesses and viscosities remain constant during the entire movement duration. Since we currently do not have enough information on the behavior of the real system during multi-joint movements, we believe that the simple model we have developed is adequate for the purpose of testing the validity of the equilibrium trajectory hypothesis. The power of the model is apparent in the fact that good

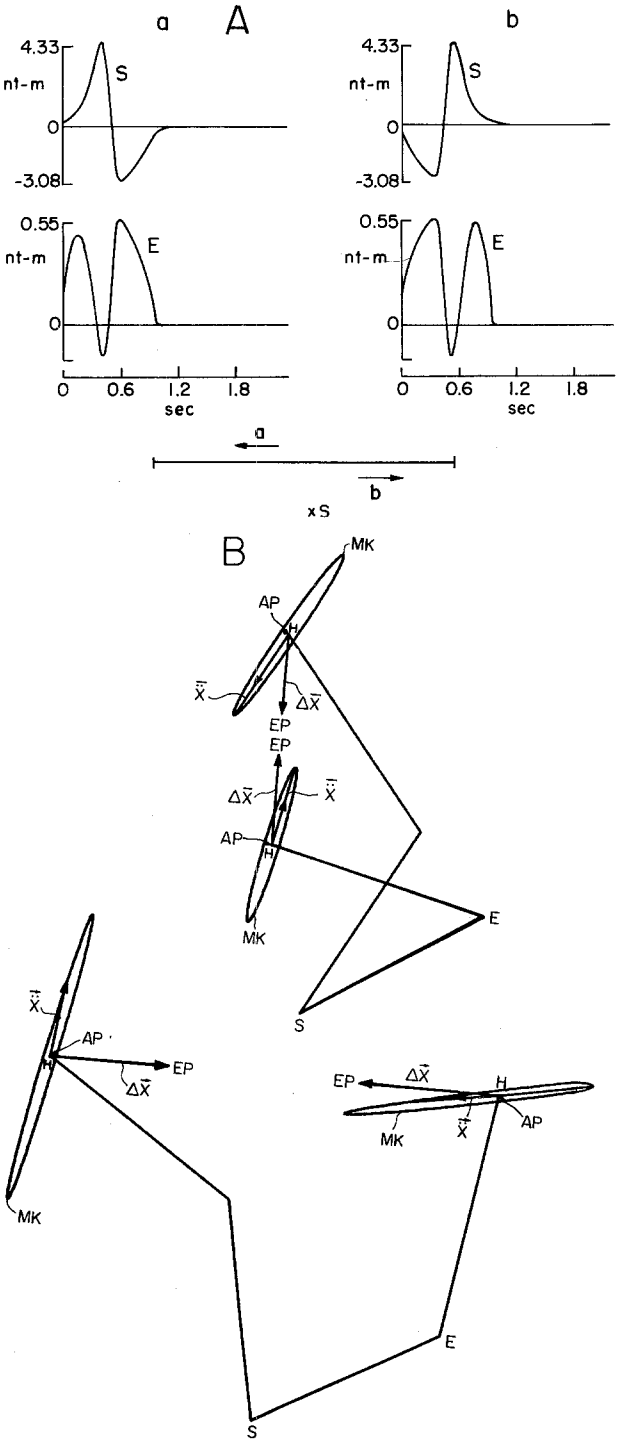

Fig. 14. **A** Profiles of shoulder (S) and elbow (E) joint torques for two movements (a and b) in two opposite directions. **B** Graphical representations of the differences between the directions of the initial hand acceleration vectors ($\ddot{\mathbf{x}}$) for movements in opposite directions. Upper illustration: movements in both directions between T_1 and T_4. Lower illustration: movements in both directions between T_2 and T_6. $\Delta\mathbf{x}$ is the displacement vector from equilibrium. AP and EP are, respectively, the actual and equilibrium hand positions at $t=0$. MK corresponds to the ellipse obtained from the multiplication of the hand stiffness matrix by the hand mobility matrix at $t=0$

quantitative agreement between the measured and simulated data was achieved here at 100 sampling points on the basis of only 4 free parameters (G_t, G_s, G_e, and ϱ). Changes introduced in the values of these parameters affected the fine details but not the qualitative features of the simulated movement curvatures.

The sensitivity analysis indicated that the best agreement with the measured trajectories can be achieved when the stiffness field has shapes and orientations similar to those observed for the static field. Our results suggest, however, that joint stiffnesses may indeed be higher during motion as compared to posture. As indicated by our results the generation of different movements might be subserved by different degrees of muscle coactivation, and during motion, the shape of the static stiffness field, at any given location, might also be slightly modified. Given the fact that the generation of different movements involves activation of different muscle groups, this is quite conceivable. The sensitivity analysis illustrated also that under AV_2 the simulated movements were straighter than both the measured movements and the movements simulated under AV_1. Moreover, to achieve good agreement with the measured data larger values for the damping coefficient had to be used in the case of whipping movements (e.g. the movement between T_2 and T_6) as compared to reaching movements (e.g. the movement between T_1 and T_4). This may suggest that the system tunes the magnitude of damping according to the estimated degree of influence of the interaction torques on the forthcoming motion. Our results, therefore, point out the importance of establishing experimentally what the actual values of the joint visco-elastic coefficients during different two-joint motions are.

However, based on the evidence presented here, we can postulate that as in posture, the dynamic elastic field also cannot be reoriented and reshaped to a degree which will allow it to fully compensate for the effects of inertial forces. The indicated limited capability of the system to modify significantly the characteristics of the dynamic stiffness field may result from coordinative constraints similar to the ones that operate during posture. Evidence for the notion that the control of posture is subserved by muscle synergies was provided by the finding that following the application of disturbance forces only the size of the elastic field significantly changed, suggesting that the activity to all arm muscles scales uniformly (Mussa-Ivaldi et al. 1985). The co-variations of the two-joint and the shoulder stiffnesses with hand position, which are responsible for the polar orientation of the stiffness field, were found to be well correlated with co-variations in the activities of the corresponding arm muscles (Flash and Mussa-Ivaldi 1984). It will be of interest, therefore, to explore, whether similar coordinative constraints also operate during arm movements. If this is the case it will mean that similar neural processes serve to translate desired positions into muscle activities during both posture and movement.

As was shown here the discrepancies between actual and equilibrium positions could be minimized if the magnitude of all joint stiffness terms could be raised by coactivating antagonist and synergistic muscle groups. Likewise, the system can use the kinematic redundancies of the human arm (Hogan 1985) in order to achieve desired end-point inertias and viscosities and to overcome the seemingly limited capability of the system to modify the position dependent characteristics of the hand stiffness field.

What strategy does the system use to change the speed of motion? It was shown above that the shape of the trajectory is preserved for movements lasting longer than 0.5 s. This implies that the same form of hand equilibrium trajectory may also underly the generation of very fast movements, not only of slow or quasistatic movements. According to Lestienne (1979) the relative durations of the activities of the agonist and antagonist muscles during elbow movements are preserved when movement speed is changed. A quadratic relation was found between peak velocity of movement and the integrated activities of these muscle groups. When muscle activation is increased, the muscle length-tension curves are shifted towards shorter rest-lengths (Rack and Westbury 1969). Taken together, these findings suggest that the equilibrium position is indeed shifted with uniformly scaled speeds. Since muscle stiffness increases with the level of activation, the higher levels of muscle activities during faster movements may be automatically associated with appropriately scaled stiffnesses. Experimental support for this hypothesis was provided by the work of Atkeson and Saund (1984).

Our data indicated, however, that at extremely high speeds the system is no longer capable of achieving precisely scaled trajectories. There are two possible reasons for this behavior. One possibility, which was considered here, is that at such high speeds the magnitudes of the joint stiffnesses and viscosities that the system is capable of generating are not adequate. We found, however, that in order to account for the observed behavior, in some cases large modifications had to be introduced in the shapes and orientations of the stiffness field. The alternative possibility is that at extremely fast movements the inertial forces dominate the dynamic behavior of the arm, since the equilibrium position is shifted in an abrupt fashion. The nature of the agonist-antagonist muscle bursts during ballistic movements (Ghez and Martin 1982) has often been mentioned (Hogan 1984; Bizzi et al. 1984) when arguing in favour of this hypothesis. Hence, further studies are needed to ellucidate the nature of hand equilibrium trajectories during very fast multi-joint arm movements.

How does the model presented here compare with alternative models for biological trajectory control? It has been recently hypothesized that trajectory control for natural arms might be achieved through computational solutions of the inverse kinematics and dynamics problems using procedures analogous to the ones used in robotics (Hollerbach 1982). Were joint torques explicitly computed and were muscles treated by the system as pure force generators there would be no apparent reason why the desired straight hand paths could not be achieved. Hence, it can be argued that at least in the case of uncontrained reaching movements, torques are not explicitly computed and are not distributed among the muscles. The system, therefore, may have adopted a simpler control strategy even at the price of movement accuracy.

As suggested by this paper, motor programs for reaching movements might be internally represented in terms of hand equilibrium trajectories in the extracorporal space. Previously it was shown that straight and curved movements in the horizontal plane can be adequately described as minimum-jerk movements, i.e. movements which maximize the smoothness of hand motion (Flash and Hogan 1985). Since minimum-jerk unconstrained reaching movements are ideally straight, the minimum-jerk description may fit hand equilibrium trajectories even better than it fits the actual movements. The work presented here therefore implies that the CNS may achieve desired behavioral goals of movements by causing the hand equilibrium position to shift along trajectories with appropriate spatial and temporal attributes. Our results also suggest that the system does not preplan a totally different hand equilibrium trajectory each time a movement is about to be generated. Instead, based on the same general motor program, and using specific information concerning the desired movement end-point locations and the desired movement duration, the system can develop a particular equilibrium trajectory plan for each individual movement.

Appendix A

If the force acting on the hand, **F**, is an explicit function of hand position **x** and if it is sufficiently differentiable in the neighborhood of the equilibrium position, then for sufficiently small displacements from equilibrium, the force displacement relationship can be assumed to be linear to a first-order approximation:

$$\mathbf{F}=K\,d\mathbf{x} \tag{A.1}$$

where K is the stiffness matrix in hand coordinates. A necessary and sufficient condition for the force to be conservative or spring-like is that $K_{xy}=K_{yx}$, i.e., that the stiffness matrix K must be a symmetric matrix.

The relation between force and displacement is the same regardless of the coordinate system in which it is represented. Based on the principle of virtual work it can be shown (Hogan 1985), that the transformation from end-point stiffness to joint stiffness is

$$R=J^TKJ \tag{A.2}$$

where J is the Jacobian matrix describing the differential transformation from joint to hand velocities. The symmetric joint-stiffness matrix due to simultaneous activity of the three different muscle groups operating on the arm is

$$R=\begin{bmatrix} R_s+R_t & R_t \\ R_t & R_e+R_t \end{bmatrix} \tag{A.3}$$

where R_s is contributed by the single-joint shoulder muscles, the stiffness coefficient R_t is mainly contributed by the two-joint muscles, and R_e is the stiffness contributed by the single-joint elbow muscles.

If $R_t=R_e=0$ and $R_s\neq 0$, the eigenvalues of the resulting hand stiffness matrix, derived from $K=J^{-T}KJ^{-1}$, are 0.0 and $R_s/l_1^2\sin^2\theta_2$. The major axis of the hand stiffness ellipse is directed along the forearm.

If $R_s=R_t=0$ and $R_e\neq 0$, the eigenvalues of the resulting hand stiffness matrix are $r^2R_e/l_1^2l_2^2\sin\theta_2$ where r is the radial distance of the hand from the shoulder. The major axis of the hand stiffness ellipse is directed along the radial axis of a polar coordinate system whose origin is located at the shoulder.

If $R_e=R_s=0$ and $R_t\neq 0$, the eigenvalues of the hand stiffness matrix are 0.0 and $R_t/l_2^2\sin^2\theta_2$ and the major axis of the hand stiffness ellipse is coaligned with the upper arm.

The differential transformations from Cartesian to polar coordinate system is

$$\begin{pmatrix} dx \\ dy \end{pmatrix}=P\begin{pmatrix} dr \\ r\,d\phi \end{pmatrix}=\begin{pmatrix} \cos\phi & -\sin\phi \\ \sin\phi & \cos\phi \end{pmatrix}\begin{pmatrix} dr \\ r\,d\phi \end{pmatrix} \tag{A.4}$$

where P is the Jacobian transformation from polar to Cartesian coordinates. Hence the transformation from end-point Cartesian to end-point stiffness expressed in polar coordinates S is

$$S=P^TKP \tag{A.5}$$

and, correspondingly, the transformation from joint stiffness to hand stiffness in polar coordinates is

$$S=P^T(J^{-T}RJ^{-1})P. \tag{A.6}$$

If $R_t=R_s$, it can be shown that

$$S=\begin{pmatrix} S_{rr} & S_{r\phi} \\ S_{\phi r} & S_{\phi\phi} \end{pmatrix}=\begin{pmatrix} \dfrac{(R_t+2R_e)}{2l_1l_2\sin^2(\theta_2/2)} & 0 \\ 0 & \dfrac{2R_t}{r^2} \end{pmatrix}. \tag{A.7}$$

This is a hand stiffness for which the principal axes of the stiffness ellipse are colinear with the axes of the polar coordinate system. Hence the stiffness ellipse has a *polar* orientation. If $l_1 = l_2$, $r = 2l_2 \cos\frac{\theta_2}{2}$ and the expression for the shape parameter of the stiffness field is

$$\frac{S_{rr}}{S_{\phi\phi}} = \left(1 + \frac{2R_e}{R_t}\right)\cot^2\frac{\theta_2}{2}. \tag{A.8}$$

Acknowledgements. This research was supported by the National Institute of Neurological Disease and Stroke Research Grant NS09343, National Institute of Arthritis, Metabolism, and Digestive Diseases Grant AM2610, and by the Advanced Research Projects Agency of the Department of Defense under Office of Naval Research Contract N00014-80-C-0505 and by a grant from the United States-Israel Binational Science Foundation (BSF), Jerusalem, Israel. The author was supported by the Bantrell Fellowship in Neurosciences.

I would like to thank Drs. Emilio Bizzi, Neville Hogan, and Ferdinando Mussa-Ivaldi, for many helpful discussions concerning the work, and for providing me with their experimental data. I wish also to thank Mr. Eric Saund for making his computer simulation programs available to me. I am also grateful to the Department of Applied Mathematics at the Weizmann Institute, where the work on this paper was completed.

References

Abend W, Bizzi E, Morasso P (1982) Human arm trajectory formation. Brain 105:331–348

Asatryan DG, Feldman AG (1965) Functional tuning of nervous system with control of movement or maintenance of a steady posture. I. Mechanographic analysis of the work of the joint on execution of a postural task. Biophysics 10:925–935

Atkeson CG, Saund E (1984) Estimation of equilibrium position, stiffness and viscosity during single joint arm movement. Neuroscience 10:335 (abstr)

Bizzi E, Polit A, Morasso P (1976) Mechanisms underlying achievement of final head position. J Neurophysiol 39:435–444

Bizzi E, Accornero N, Chapple W, Hogan N (1982) Arm trajectory formation. Exp Brain Res 46:139–143

Bizzi E, Accornero N, Chapple W, Hogan N (1984) Posture control and trajectory formation during arm movement. J Neurosci 4:2738–2744

Cannon S, Zahalak GI (1982) The mechanical behavior of active human skeletal muscle in small oscillations. J Biomech 15:111–121

Feldman AG (1966) Functional tuning of nervous system with control of movement or maintenance of a steady posture. II. Controllable parameters of the muscle. Biophysics 11:565–578

Feldman AG (1974) Change in the length of the muscle as a consequence of a shift in equilibrium in the muscle-load system. Biophysics 19:544–548

Feldman AG (1980) Superposition of motor programs. I. Rhythmic forearm movements in man. Neuroscience 5:81–90

Flash T, Hogan N (1985) The coordination of arm movements: an experimentally confirmed mathematical model. J Neurosci 7:1688–1703

Flash T, Mussa-Ivaldi FA (1984) Inferring movement and muscle synergies from multi-joint arm posture. Neuroscience 10:635 (abstr)

Georgopoulos AP (1986) On reaching. Annu Rev Neurosci 9:147–170

Ghez C, Martin JH (1982) The control of rapid limb movement in the cat. III. Agonist-Antagonist coupling. Exp Brain Res 45:115–125

Gielen CCAM, Houk JC (1984) Nonlinear viscosity of human wrist. J Neurophysiol 52:553–569

Hallett M, Marsden CD (1979) Ballistic flexion movements of the human thumb. J Physiol 294:33–50

Hatze H (1979) A model for the computational determination of parameter values of anthropomorphic segments. South African C.S.I.R. Technical Report TWISK 79

Hoffer JA, Andreassen S (1981) Regulation of soleus muscle stiffness in premammillary cats: intrinsic and reflex components. J Neurophysiol 45:267–285

Hogan N (1984) An organizing principle for a class of voluntary movements. J Neurosci 4:2745–2754

Hogan N (1985) The mechanics of multi-joint posture and movement. Biol Cybern 52:315–331

Hollerbach JM (1982) Computers, brains and the control of movement. Trends Neurosci 5:189–192

Hollerbach JM, Flash T (1982) Dynamic interactions between limb segments during planar arm movement. Biol Cybern 44:67–77

Joyce GC, Rack PMH, Westbury DR (1969) The mechanical properties of cat soleus muscle during controlled lengthening and shortening movements. J Physiol 204:461–474

Kelso JAS, Holt KG (1980) Exploring a vibratory systems analysis of human movement production. J Neurophysiol 43:1183–1196

Lacquaniti F, Licata F, Soechting JF (1982) The mechanical behavior of the human forearm in response to transient perturbations. Biol Cybern 44:35–46

Lestienne F (1979) Effects of inertial load and velocity on the bracking process of voluntary limb movement. Exp Brain Res 35:407–418

MacKay WA, Crammond DJ, Kwan HC, Murphy JT (1986) Measurements of human forearm viscoelasticity. J Biomech 19:231–238

Morasso P (1981) Spatial control of arm movements. Exp Brain Res 42:223–227

Mussa-Ivaldi FA, Hogan N, Bizzi E (1985) Neural, mechanical and geometric factors subserving arm posture in humans. J Neurosci 5:2732–2743

Nichols TR, Houk JC (1976) Improvement in linearity and regulation of stiffness that results from actions of stretch reflex. J Neurophysiol 39:119–142

Polit A, Bizzi E (1979) Characteristics of motor programs underlying arm movements in monkeys. J Neurophysiol 42:183–194

Rack PMH, Westbury DR (1969) The effects of length and stimulus rate on tension in the isometric cat soleus muscle. J Physiol 204:443–460

Received: August 18, 1986

Dr. Tamar Flash
Department of Applied Mathematics
The Weizmann Institute of Science
Rehovot 76100
Israel